Utah State University

DigitalCommons@USU

Space Dynamics Lab Publications

Space Dynamics Lab

1-1-1995

Stray Light Analysis of the SABER Telescope

John Stauder

Roy Esplin

Lorin Zollinger

Marty Mlynczak

Jim Russell III

Larry Gordley

See next page for additional authors

Follow this and additional works at: https://digitalcommons.usu.edu/sdl_pubs

Recommended Citation

Utah State University
MERRILL-CAZIER LIBRARY

Authors

John Stauder, Roy Esplin, Lorin Zollinger, Marty Mlynczak, Jim Russell III, Larry Gordley, and Tom Marshall

Stray light analysis of the SABER telescope

John Stauder, Roy Esplin, Lorin Zollinger
Space Dynamics Laboratory/Utah State University
1695 North Research Park Way, Logan, UT 84341

Marty Mlynczak and Jim Russell III
NASA Langley Research Center
Hampton, VA 23681

Larry Gordley and Tom Marshall
GATS Inc.
28 Research Drive, Hampton, VA 23666

ABSTRACT

The stray light analysis of the sounding of the atmosphere using broadband emission radiometry (SABER) instrument on the thermosphere-ionosphere-mesosphere energetics and dynamics (TIMED) mission is discussed. Relevant mission objectives and operating conditions are stated to define the stray light problem. Since SABER is an earth limb viewing sensor, the telescope must be designed for large off-axis rejection. Described are the key design features which make the instrument well suited for its mission. Representative point source transmittance (PST) curves computed using the commercial stray light program APART are presented. Non-rejected radiance (NRR) values computed using APART generated PST curves and LINEPACK generated curves for the total radiance from the earth and the atmosphere are given. A method for computing NRR from the earth and the atmosphere using line-of-sight radiance profiles versus tangent height is described. Computed NRR values demonstrate that the effect of stray light on SABER's measurement capability is negligible.

Keywords: APART, LINEPACK, PST, SABER, TIMED, stray light, non-rejected radiance, point source transmittance

1. INTRODUCTION

The SABER instrument is part of the TIMED mission scheduled for launch in 1998. The sensor is a follow-up to the LIMS instrument which flew on Nimbus 7, however, SABER's sensitivity is expected to be 30 times that of LIMS. This paper discusses the stray light design features and analysis of the SABER instrument.

SABER has stringent requirements for the rejection of off-axis earth and atmospheric radiation which are driven by the fact that SABER is designed to observe limb emission primarily from the mesosphere and lower thermosphere, 50 to 150 km in tangent height. The radiance levels from this region of the atmosphere are generally quite small relative to the radiances from the denser lower atmosphere and from the hard earth surface. Thus even small amounts of non-rejected, off-axis radiation could seriously compromise the SABER science measurements.

2. INSTRUMENT OVERVIEW

The instrument objectives and parameters of SABER that are helpful in defining the stray light problem are given below. The instrument is described in greater depth in a companion paper.[1]

The SABER instrument is a 10-channel earth limb viewing sensor that is to measure atmospheric emissions

Table 1. SABER Spectral passbands & noise equivalent radiances

Channel Number	Channel Name (Based on atmospheric species measured)	Spectral Passband (μm)	NER (Wcm^{-2}sr^{-1})
1	CO_2 - N	14.888 - 15.520	1.70E-8
2	CO_2 - W	13.347 - 16.941	2.80E-8
3	CO_2 - W	13.347 - 16.941	2.80E-8
4	O_3	9.057 - 9.729	1.10E-8
5	H_2O	6.510 - 7.120	3.70E-9
6	NO	5.257 - 5.566	2.50E-9
7	CO_2 - B	4.197 - 4.350	1.30E-9
8	OH - A	1.952 - 2.189	4.70E-10
9	OH - B	1.562 - 1.698	4.70E-10
10	O_2	1.262 - 1.285	4.70E-10

in the 1 to 17 μm spectral range. The telescope, shown in Figure 1, is an on-axis design with a 52% central obscuration. The focal length is 200 mm and the f-number is 2. The earth limb is scanned vertically using a single axis scan mirror. The incoming light is limited by the aperture stop located at the primary mirror. A chopper that also functions as an intermediate or first field stop is located at the cassegrain focus. The light is then refocused onto the focal plane by reimaging optics consisting of two mirrors. The window is used to protect the filter and detector assemblies from contamination. The focal plane assembly consists of an array of 10 discrete detectors covered by 10 passband filters. The spectral passbands and the required noise equivalent radiance (NER) values for each channel are tabulated in Table 1. Channels 2 and 3 have identical spectral passbands; because of their different locations on the focal plane they have different fields of view and consequently provide a means for correcting spacecraft pointing variations.
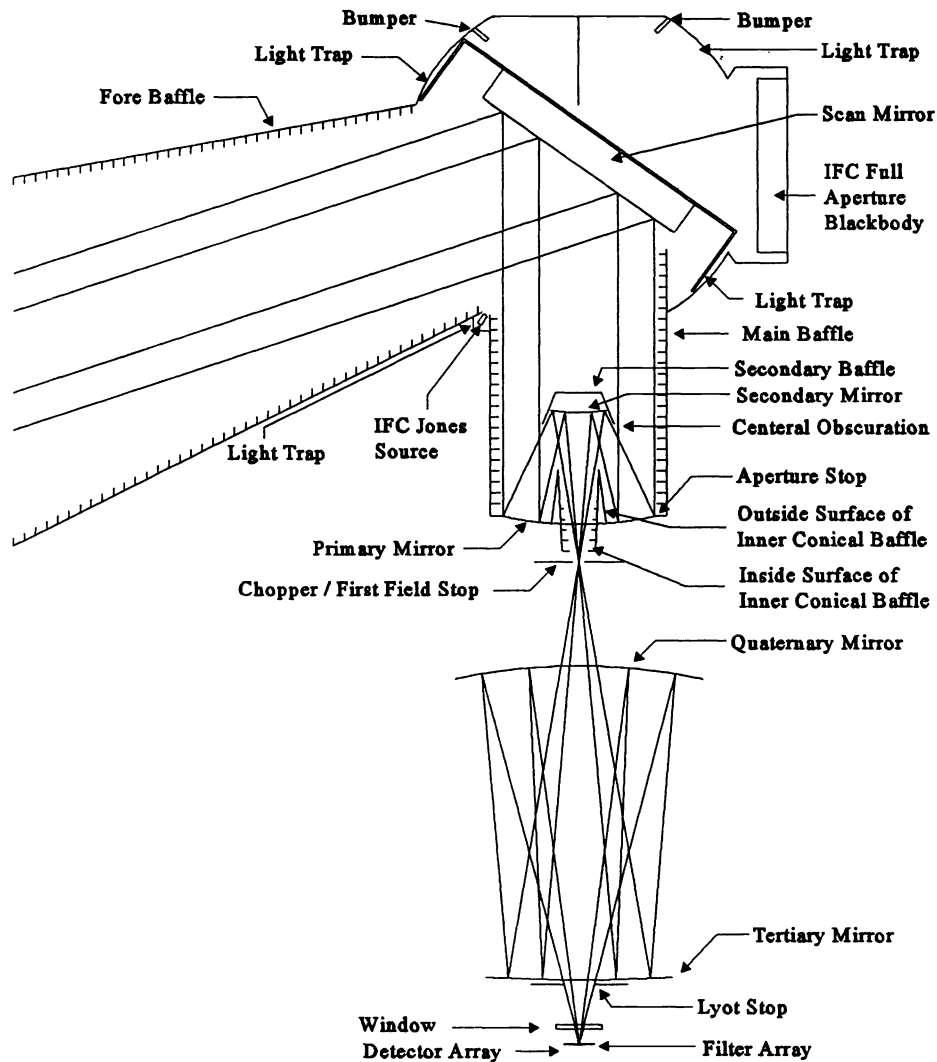

Figure 1. SABER optical system

3. STRAY LIGHT DESIGN FEATURES

The reimaging optics of SABER allow for the use of two important design features, an intermediate field stop and a Lyot (glare) stop. The field stop blocks direct radiation, i.e. specular rays, from off-axis sources. Only scattered light from the mirrors, baffles, and mechanical elements located prior to the intermediate stop are allowed to enter the reimaging part of the system. Scattered light from these components are reduced as follows: First, the scan, primary, and secondary mirrors are superpolished. Second, a fore baffle

is used to minimize the angles that the mirrors can be directly illuminated by off-axis sources. Next, the vane depth and spacing of the fore and main baffles are chosen to optimally trap incident radiation. Finally, the baffle vanes and remaining non-optical elements are coated with a highly absorptive paint. The other major design feature which suppresses stray light is the use of a cold Lyot stop placed conjugate with the entrance aperture stop located at the primary mirror. This stop removes diffracted light from the edge of the aperture stop and direct scatter from the baffles. The cold Lyot stop also limits the infrared background radiation from within the telescope.

4. INSTRUMENT STRAY LIGHT PERFORMANCE

Stray light is the unwanted radiation that reaches a sensor's detector. Unwanted radiation is defined as any radiation that is outside the desired field of view of the sensor. The two main sources of stray light for SABER are the thermally emitted radiation from the earth's surface and emissions from the atmosphere. Other sources include reflected sunlight, or albedo, and thermally emitted radiation from within the telescope. Several paths exist where radiation from these off-axis sources can reach the detector. They include scattered radiation from optical and non-optical surfaces, diffraction from sharp edges such as the entrance port edge, and direct illumination as can be the case with internal thermal emissions.

Thermal emissions from SABER components located in front of the chopper are neutralized by subtracting the instrument response to deep space (the instrument zero-signal response) from each earth-limb measurement. Thermal emissions from components after the chopper add nothing to the signal because they are unchopped. Thus, to first-order accuracy, thermal emissions from SABER itself are not confused with signal, however they do contribute to the photon noise. So far this photon noise contribution has been bounded using first-order techniques, and it is included in the NER values tabulated in Table 1. An APART analysis to refine this estimate is planned for next year. Thermal emissions from within SABER are not considered further in this paper.

The stray light analysis was performed using the APART[2] program from Breault Research Organization, Inc. The dominate stray light paths to the detector are scatter from the scan, primary, and secondary mirrors. Minor stray light paths include diffraction from the intermediate field stop and Lyot stop edges, and scattered radiation off of the tertiary and quaternary mirrors. A useful output of APART is the sensor's off-axis response to a point source which is discussed below.

The off-axis response of SABER is described by the point source transmission (PST) curve. The PST curve shown in Figure 2 (solid line) is for channel 3 with a field-of-view tangent height of 100 km. The PST is defined as the power on the detector, as a function of a point source's off-axis angle, normalized by the detector power from the point source on-axis, or

$$PST(\theta) = \frac{P_d(\theta)}{P_d(0^\circ)} \tag{1}$$

SABER's PST can be interpreted as follows: At off-axis angles less than 5°, scattered light off of the primary and secondary mirrors that is imaged onto the detector dominates. Scattered radiation from the scan mirror reaching the detector becomes significant at 5° and dominates by 15°. The response steadily decreases with increasing off-axis angles until the scan mirror becomes totally shielded from the point source by the fore baffle. This is indicated by the rapid drop in the response after 22°. Multiple scattering paths involving the scan mirror account for the remaining off-axis response. These paths include diffraction from the entrance port edge and scatter from the fore baffle knife edges which in turn scatter off the scan mirror onto the detector. The
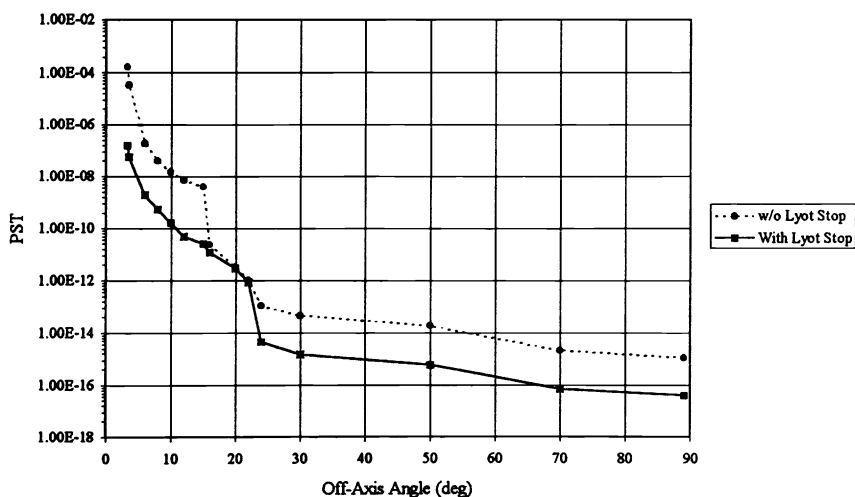

Figure 2. SABER PST curves with and without Lyot stop

steady decline in the response after 22° results from the decrease in illumination of the entrance port edge and fore baffle.

To illustrate the importance of the Lyot stop, this design feature was removed from the analysis. The resulting PST curve is also shown in Figure 2 (dashed line). Except for the region from 16° to 22°, the off-axis response is more than an order of magnitude better when the Lyot stop is utilized. In fact, at angles less than 5° the response is three orders of magnitude better. The reason for the improved performance is that the Lyot stop blocks all of the scattered and diffracted radiation from the aperture stop and aperture stop edge, respectively. So what happens in the 16° to 22° region? At 16° the fore baffle shields the aperture stop from the point source, thus reducing the benefits of the Lyot stop. Scan mirror scatter dominates in this region. After 22°, the advantages of the Lyot stop are again realized as multiple scattering paths from the aperture stop are blocked.

5. NON-REJECTED RADIANCE

The non-rejected radiance (NRR) from the earth and the atmosphere was computed as SABER's field of view was scanned across the earth limb by rotating the scan mirror. The earth-sensor geometry is illustrated in Figure 3, where $x_1 y_1 z_1$ is the sensor coordinate system, and the $x_2 y_2 z_2$ coordinate system defines the nadir ($-z_2$) and the local horizon (y_2). NRR values were computed using the following integral

$$NRR = \frac{2}{\Omega} \int_{-\frac{\pi}{2}}^{\frac{\pi}{2}} \int_{0}^{\frac{\pi}{2}} PST(\theta) L(h(\theta,\phi)) \sin(\theta) d\theta d\phi \quad (2)$$

where the variables of integration θ and ϕ are the polar and azimuthal angles of the senor as defined in the bubble in Figure 3, PST is the point source transmittance function, L is the is the line-of-sight radiance from the earth and the atmosphere, and Ω is the solid angle of the sensor field of view. PST functions were computed for each scan mirror angle and each channel using APART. As is often done, the above integral assumes PST values are symmetrical about the baffle axis; that is, they are independent of the azimuthal angle ϕ. Radiance values are assumed to be symmetrical about the center of the earth so they are completely determined by the tangent height. As can be seen from Figure 3, the tangent height as a function of the variables of integration can be computed using the following equations

$$\mathbf{v} = \begin{bmatrix} 0 \\ 0 \\ -(s + R) \end{bmatrix} \quad (3)$$

$$\mathbf{u}(\theta,\phi) = \begin{bmatrix} \sin(\theta)\cos(\phi) \\ -\sin(\theta)\sin(\phi)\sin(\alpha) + \cos(\theta)\cos(\alpha) \\ -\sin(\theta)\sin(\phi)\cos(\alpha) - \cos(\theta)\sin(\alpha) \end{bmatrix} \quad (4)$$

$$r(\theta,\phi) = \mathbf{u}(\theta,\phi) \cdot \mathbf{v} \quad (5)$$

$$\mathbf{w}(\theta,\phi) = \mathbf{v} - r(\theta,\phi)\mathbf{u}(\theta,\phi) \quad (6)$$

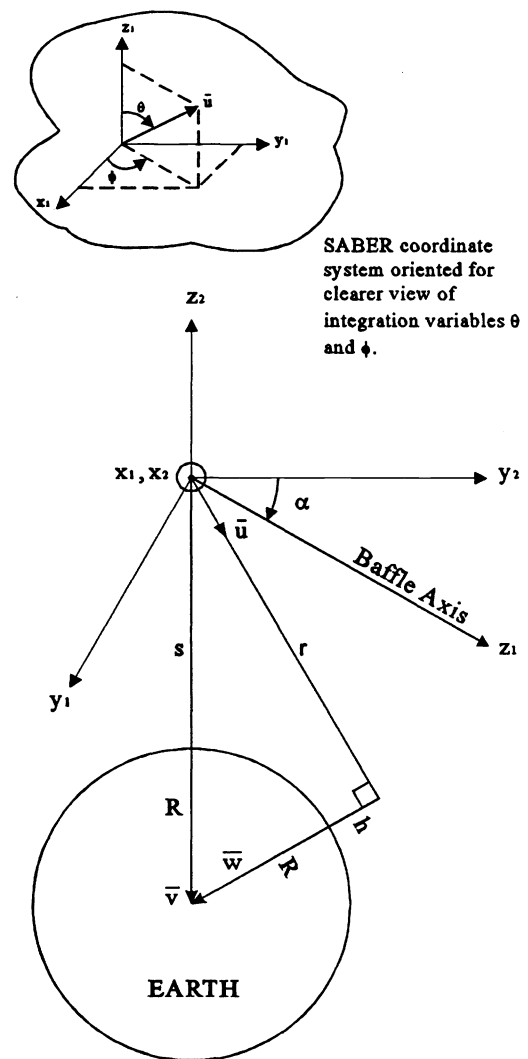$$h(\theta,\phi) = |\mathbf{w}(\theta,\phi)| - R \quad (7)$$

SABER coordinate system oriented for clearer view of integration variables θ and ϕ.

Figure 3. Geometry of non-rejected radiance integration

where, v is the nadir vector, u is the unit vector in the direction defined by the integration variables θ and ϕ, w is the vector orthogonal to the line containing u to the center of the earth, s is the orbit height, α is the baffle depression angle (18.658°), R is the radius of the earth and r is the range from the sensor to the measurement point at tangent height h. Since the nadir vector v passes through the center of the earth and since the earth and atmosphere are assumed to be symmetrical about the center of the earth, the radiance in any direction u can be specified as a function of tangent height if the definition of tangent height is expanded to include negative values for those cases when the length of vector w is less than the radius of the earth. Thus when the line containing u intersects the earth, the tangent height h is negative and the line-of-sight radiance depends on earth emission, atmospheric emissions and atmospheric absorption.

Line-of-sight radiance values for both negative and positive tangent heights were computed using the line-by-line radiance code LINEPAK described in Gordley et. al.[4] Fundamental to this computation is the ability to accurately calculate the atmospheric radiance for a variety of transitions that are not in local thermodynamic equilibrium (LTE). In some transitions, such as the $O_2(^1\Delta)$ transition at 1.27 μm and the $O_3(\nu_3)$ transitions at 9.6 μm, the electronic or vibrational temperatures greatly exceed the kinetic temperature, while other transitions such as the NO(v) at 5.3 μm and the $CO_2(\nu_2)$ transitions at 15 μm generally have vibrational temperatures less than the kinetic temperature. It is therefore critical to have the correct emission physics in this atmospheric region to assess the impact of stray light. A radiance calculation assuming LTE would greatly overestimate or underestimate the actual radiance, depending on the SABER channel. The specific non-LTE conditions used in the SABER study can be found in the paper by Mlynczak et al[5] and references therein. So far radiance profiles versus tangent height have only been generated for channels 1,2,3,4,6 and 10. This subset of channels is representative of SABER's performance because it includes the long wavelength CO_2 channels, the ozone channel, the mid wavelength NO channel and the shortest wavelength O_2 channel. Night-time conditions were assumed in computing radiance profiles for the CO_2, O_3, and the NO channels. However since the sun's effect is negligible for these channels, the resulting values also represent day-time emission values. The NRR contribution of the earth's albedo was found to be negligible for these channels by using APART to compute the NRR for an albedo of 0.44. The maximum albedo NRR contribution was 4% for the NO channel. Day-time emission rates were used in the computation of the O_2 radiance profiles because the solar excitation is significant for this channel. The albedo contribution to the NRR for the O_2 was computed using APART and added to the NRR value computed using the integral in Equation 2. The contribution from the earth's albedo and out of field atmospheric emissions are approximately equal for the O_2 channel.

The computed NRR values normalized by the NER are plotted as a function of field-of-view tangent height in Figure 4. The NRR
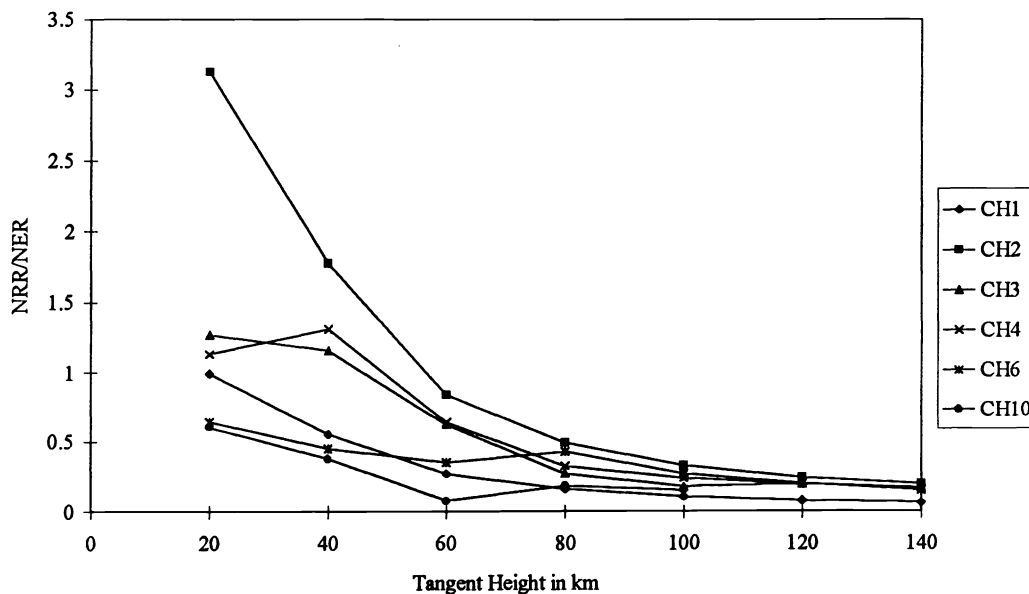

Figure 4. Normalized non-rejected radiance

is negligible above tangent heights of 60 km for all channels since it is less than 1 NER. Below 60 km the NRR for some channels is more than 1 NER, but the percentage of signal due to NRR actually decreases below 60 km as shown in Figure 5. As can be seen from this figure, NRR is less than 0.2% for tangent heights less than 60 km for all channels except the NO channel. The larger NRR percentage values for this channel are not due to stray light problems but rather are due to the weak emissions in this channel. The sensitivity of this channel would have to be improved to benefit from a better stray light design since for this channel NRR is less than 1 NER for all tangent heights. For the other four channels the percentage increase above 60 km is due to decreasing signal since the stray light input is decreasing with tangent height as shown in Figure 4. These computed NRR values verify the suitability of the SABER stray light design because the effects of stray light on SABER's measurement capability are negligible.
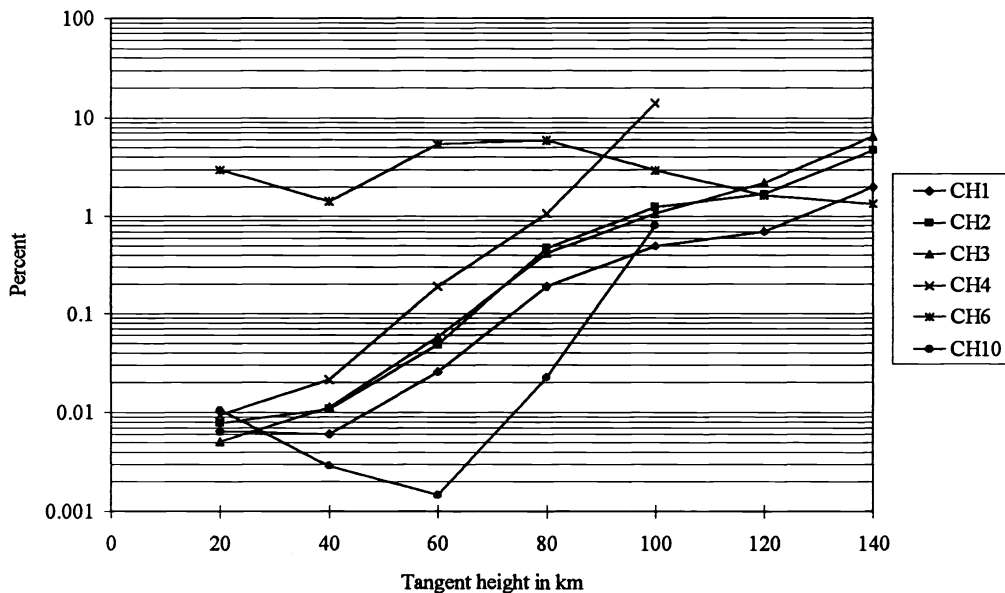

Figure 5. Percent of signal due to stray light

6. CONCLUSIONS

The SABER design allows for the effective use of stray light suppression features. These design features include an intermediate field stop and a Lyot stop. Point source transmittance curves were computed using APART for 6 of SABER's 10 channels at scan mirror angles corresponding to field-of-view tangent heights ranging from 20 to 140 km. The dominant stray light contributors to the non-rejected radiance from the earth and atmosphere are scatter from the scan, primary and secondary mirrors. A method was described for computing non-rejected radiance from both the earth and the atmosphere by extending the definition of tangent height to include negative values. For negative tangent heights the line-of-sight intercepts the earth and the radiance depends on earth and atmospheric emissions as well as atmospheric absorption. Radiance profiles were computed using the line-by-line radiance code LINEPAK. Curves of non-rejection radiance computed using this method indicate that stray light will not affect SABER's measurement capability.

7. REFERENCES

1. Esplin, R., *et. al.*, "SABER Instrument Design Update," *SPIE Proceedings,* Vol. 2553, 1995

2. "APART Stray Light Analysis Software Package, Version 9.3," Breault Research Organization, 6400 East Grant Road, Suite 350, Tucson, Arizona, 85715.

3. Mlynczak, M. G., D. S. Zaras, and M. Lopez-Puertas, "Rapid computation of spectrally integrated non-LTE limb emission," *J. Geophys. Res.*, 99, 25761-25772, 1994.

4. Gordley, L.L., B. T. Marshall, and D. A. Chu, "LINEPAK: Algorithm for modeling spectral transmittance and radiance," *J. Quant. Spectrosc. Radiat. Transfer*, 52, 563-580, 1994.